Multi-pass Cooperative Near-Field and Far-Field ISAC Energy Efficiency Optimization

Feiyang Yu
School of Computer Science, Zhejiang University of Technology, Hangzhou 310023, Zhejiang, China
Corresponding author: Feiyang Yu (e-mail: 19857182506@163.com)

ABSTRACT In the recent past, Pinching Antenna Systems (PASS) have gained popularity because of their flexible deployment strategies and efficient link gain performance. This study presents a novel integrated sensing and communication (ISAC) system assisted by multiple flexible RF feedlines (or tracks) and multiple active Reconfigurable Intelligent Surfaces (RIS) to optimize real-time monitoring and data transmission across automated production lines. The proposed ISAC system includes a communication energy efficiency maximization problem subject to the sensing Signal-to-Noise Ratio (SNR) and power budget constraints. The resulting optimization problem is solved by employing an alternating optimization strategy to reformulate the original problem into three tractable sub-problems: the PASS antennas optimization problem, the digital beamforming problem, and the active RIS reflection matrix problem. The three original problems are then solved by utilizing methods that involve Fractional Programming, the Penalty Function Method, and the Element-wise Optimization strategy, respectively. Simulation outcomes show a significant improvement in both energy efficiency and sensing performance for the novel strategy compared to the Multiple-Input Multiple-Output (MIMO) and the Passive RIS-Assisted PASS system. Specifically, the proposed scheme achieves up to 166.7% higher energy efficiency than the conventional MIMO-ISAC baseline under identical power budgets and interference constraints.

INDEX TERMS Integrated Sensing and Communication (ISAC); Pinching Antenna System (PASS); Multiple Active Reconfigurable Intelligent Surfaces (RIS); Energy Efficiency Optimization.

I. INTRODUCTION

A. BACKGROUND

With the advancement of sixth-generation (6G) wireless networks, Integrated Sensing and Communication (ISAC) has emerged as a pivotal technology for driving the digital transformation of the industry through the deployment of intelligent, fiber-integrated sensing fabrics. From a spectrum perspective, improvements in communication capacity and sensing performance are both contingent upon larger bandwidth availability, which further exacerbates the pressure on limited spectrum resources. Consequently, how to effectively improve spectral efficiency under bandwidth-constrained conditions has become a critical issue that urgently needs to be addressed. In recent years, novel reconfigurable wireless technologies, including Reconfigurable Intelligent Surfaces (RIS) [1], Movable Antennas (MAs) [2], and Fluid Antennas (FAs) [3], have garnered extensive attention from both academia and industry. These technologies can significantly improve channel conditions by proactively shaping the wireless propagation environment, effectively enhancing spectral efficiency within smart systems where conductive fibers and fabric structures influence signal interaction.

B. RELATED WORK

Reconfigurable Intelligent Surfaces consist of a large number of active or passive programmable reflecting elements, which reshape the wireless propagation environment by adjusting their phase responses, thereby demonstrating significant advantages in enhancing channel capacity, extending coverage range, and reducing power consumption. In recent years, extensive research efforts have been devoted to RIS-assisted Integrated Sensing and Communication (ISAC) systems [4–6]. In this context, the work in [7] addressed scenarios where the direct link is obstructed by leveraging RIS to establish controllable reflection paths for restoring communication link quality, and further designed optimization strategies to enhance the sensing performance of the system. The study in [8] incorporated RIS into multi-user ISAC architectures, optimizing the reflection coefficients to suppress multi-user interference while preserving the desired sensing beampattern characteristics. It is noteworthy that the aforementioned works are all based on passive RIS architectures. In contrast, [9] embedded active amplifiers within the reflecting elements and revealed the advantages of active RIS over passive RIS in terms of link gain under multiplicative fading environments. Furthermore, studies in [10] and [11] have validated that deploying active RIS in ISAC systems can significantly enhance both communication and sensing performance. However, these investigations primarily focused on system designs involving a single active RIS, while systematic exploration of the cooperative mechanisms among multiple RIS and their potential gains in ISAC remains insufficient.

II. SYSTEM MODEL

A. LOCATION MODELING

As illustrated in Fig. 1, this paper investigates an Integrated Sensing and Communication (ISAC) downlink system jointly assisted by a Pinching Antenna System (PASS) and multiple Reconfigurable Intelligent Surfaces. Formally, a PASS is defined as a reconfigurable antenna array integrated with a metallic waveguide, where the "pinching" mechanism allows for the dynamic adjustment of antenna positions to optimize beamforming and interference nulling, effectively acting as a form of liquid or movable antenna (MA) system [2], [3] within a constrained physical track.

The Base Station (BS) transmits probing signals toward sensing targets through movable antennas distributed along the low-loss flexible feedlines, while simultaneously providing downlink communication services to single-antenna communication users in the system. The system comprises two categories of communication users: near-field users and far-field users, where the boundary is determined by the frequency-dependent Fraunhofer distance (Rayleigh distance) $d = 2D^2/\lambda$. This ensures that the categorization is not a static geographic boundary but adapts to the operational frequency and aperture size. Since the locations of far-field users exceed the effective coverage area of PASS and reside in the radiative far-field region, their downlink transmission primarily relies on the reflection paths provided by active RIS deployed at the edge of PASS for enhancement. The active RIS is specifically integrated to compensate for the severe multiplicative fading experienced by far-field users, which is not required for near-field links. In contrast, near-field users are located within the Fresnel coverage range of PASS and receive downlink signals from the BS directly through PASS. The necessity of handling the "near-field sensing target" solely via PASS stems from the inherent high-resolution beam-focusing capabilities of PASS in the near-field, which provides sufficient gain without the added hardware complexity and thermal noise of an active RIS.

Near-field region: This region comprises K communication users and a target user designated for sensing task execution. The set of communication users is denoted as $\mathcal{K}_{\text{near}}$ and the sensing target is denoted as m. Let $\mathbf{I}_k$ represent the position of the k-th near-field communication user, and $\mathbf{I}_m$ denote the position of the near-field sensing user m. Their respective positions in the two-dimensional plane are given by

$$\mathbf{I}_k = [x_k, y_k, 0]^T, \quad \forall k \in \mathcal{K}_{\text{near}}, \tag{1}$$

$$\mathbf{I}_t = [x_t, y_t, 0]^T. \tag{2}$$

Far-field region: Due to the inherent difficulty for far-field users to acquire reliable signals directly from the base station or PASS waveguide, the system deploys an active reconfigurable intelligent surface (RIS) comprising R elements for each far-field user to enhance communication coverage. This active RIS serves to receive the signals radiated from the base station, amplify them, and subsequently reflect them directionally toward the designated user.

To mitigate self-interference between the transmit and receive links, the system employs a separated waveguide architecture: downlink communication and sensing signals are transmitted through N transmit RF tracks, while the echo signals reflected from the target are collected by an independent receive track. To ensure real-time movement and impedance matching, each track incorporates a non-contact sliding feed mechanism (e.g., capacitive coupling), allowing antennas to shift positions without compromising the RF feed integrity. Each transmit waveguide is equipped with M pinching antennas, where $\mathcal{N}$ and $\mathcal{M}$ denote the index sets of transmit waveguides and pinching antennas, respectively. The input ports of all transmit waveguides are connected to the base station radio frequency chain through an in-phase feeding network, thereby ensuring phase and amplitude consistency of the fed signals across all waveguide ports.

All waveguides are assumed to extend along the x-axis direction, positioned at a height of d_h, and arranged in a linear array along the y-direction with an inter-waveguide spacing of y_n. The feeding point position of the n-th waveguide is expressed as

$$\mathbf{I}_n = [D, y_n, d_n]^T, \quad n \in \mathcal{N}, \tag{3}$$

while the position of the m-th pinching antenna (PA) on the waveguide is given by

$$\mathbf{I}_m^n = [x_{n,m}, y_n, d_h]^T, \quad n \in \mathcal{N},\ m \in \mathcal{M} \tag{4}$$

To avoid mutual interference between adjacent PAS, the x-axis positions must satisfy

$$0 \le x_{n,m} \le L, \quad x_{n,m} - x_{n,m-1} \ge \delta \tag{5}$$

where L denotes the waveguide length and δ represents the minimum inter-antenna spacing. Accordingly, the set of x-coordinate positions for all transmit PAS can be expressed as

$$\mathcal{X} = \{x_{n,m} \mid 0 \le x_{n,m} \le L,\ x_{n,m} - x_{n,m-1} \ge \delta,\ \forall n, m\} \tag{6}$$

The receive waveguide comprises M receive PAS, whose corresponding positions are denoted as

$$\bar{\mathbf{I}}_{m,r} = [x_r, y_r, d_h]^T$$

where the set of positions constituted by $\mathbf{X}_r$ is defined as $\mathcal{X}_r$.

B. CHANNEL MODELING

The wireless channel between the PA on the n-th waveguide and the k-th near-field user can be expressed as

$$\mathbf{h}_k^n = (2\kappa_c)^{-1}\left[\frac{e^{-j\kappa_c r_{k,1}^n}}{r_{k,1}^n}, \frac{e^{-j\kappa_c r_{k,2}^n}}{r_{k,2}^n}, \ldots, \frac{e^{-j\kappa_c r_{k,M}^n}}{r_{k,M}^n}\right]^T \tag{7}$$

where $\kappa_c = 2\pi f_c/c = 2\pi/\lambda_c$ denotes the wavenumber, and $r_{k,m}^n = \|\mathbf{I}_m^n - \mathbf{I}_k\|_2$ represents the distance between the m-th PA on the n-th waveguide and user k.

Furthermore, the overall wireless channel vector between all PAS and user k can be expressed as

$$\hat{\mathbf{h}}_k = \left[(\mathbf{h}_k^1)^T, (\mathbf{h}_k^2)^T, \ldots, (\mathbf{h}_k^N)^T\right]^T \in \mathbb{C}^{MN\times 1} \tag{8}$$

Similarly, the channel vector between PA and the target on the N-th waveguide is

$$\mathbf{h}_t^n = (2\kappa_c)^{-1}\left[\frac{e^{-j\kappa_c r_{t,1}^n}}{r_{t,1}^n}, \frac{e^{-j\kappa_c r_{t,2}^n}}{r_{t,2}^n}, \ldots, \frac{e^{-j\kappa_c r_{t,M}^n}}{r_{t,M}^n}\right]^T, \tag{9}$$

where $r_{t,m}^n = \|\mathbf{I}_m^n - \mathbf{I}_t\|_2$. The channel between all PAS and the sensing user can be formulated as [12]

$$\hat{\mathbf{h}}_t = \left[(\mathbf{h}_t^1)^T, (\mathbf{h}_t^2)^T, \ldots, (\mathbf{h}_t^N)^T\right]^T \in \mathbb{C}^{MN\times 1} \tag{10}$$

Since the propagation loss within the RF feedline is substantially lower than the attenuation experienced during free-space propagation, this paper neglects the power attenuation inside the feedline and considers only the effect of propagation delay. Consequently, the internal waveguide channel matrix can be expressed as

$$\mathbf{F} = \mathrm{Bdiag}(\mathbf{f}_1, \mathbf{f}_2, \ldots, \mathbf{f}_N)^T \in \mathbb{C}^{N\times MN} \tag{11}$$

where $\mathbf{f}_n = [f_1^n, f_2^n, \ldots, f_M^n]^T \in \mathbb{C}^{M\times 1}$. The element f_m^n denotes the phase difference between the output signal and the input signal of the m-th PA on the n-th waveguide, which is specifically given by

$$f_m^n = \rho_m^n e^{-j\kappa_g d_m^n} \tag{12}$$

where $\kappa_g = 2\pi/\lambda_g$ denotes the waveguide propagation wavenumber, $\lambda_g = \lambda_c/n_e$ represents the guided wavelength, n_e is the effective refractive index of the waveguide, $d_m^n = \|\mathbf{I}_n - \mathbf{I}_m^n\|_2$ denotes the distance between the feeding point of the n-th waveguide and its m-th PA, and ρ_m^n represents the power allocation coefficient of the corresponding PA.

To simplify the analysis, an equal power allocation strategy is assumed within each waveguide. Under this assumption, the overall equivalent channel between the base station and the k-th user, as well as the equivalent channel between the base station and target m, can be expressed as

$$\mathbf{h}_{u,k} = \mathbf{F}\hat{\mathbf{h}}_k \in \mathbb{C}^{N\times 1}, \quad \mathbf{h}_{t,m} = \mathbf{F}\hat{\mathbf{h}}_t \in \mathbb{C}^{N\times 1} \tag{13}$$

Similarly, the equivalent channel from the sensing target to the base station can be expressed as

$$\mathbf{h}_{r,m} = \mathbf{f}_{r,m}^H \hat{\mathbf{h}}_{r,m} \in \mathbb{C}^{1\times N} \tag{14}$$

where $\hat{\mathbf{h}}_{r,m}$ and $\mathbf{f}_{r,m}$ represent the channel from the user to the receive waveguide and the internal channel vector of the receive waveguide, respectively. In the BS-RIS link, let the PASS-RIS matrix be denoted as $\hat{\mathbf{H}}_{\mathrm{RIS}}$. Then the overall channel from the base station to the r-th RIS can be expressed as

$$\tilde{\mathbf{H}}_r = \mathbf{F}\hat{\mathbf{H}}_{\mathrm{RIS}} \in \mathbb{C}^{N\times R} \tag{15}$$

C. SIGNAL MODEL

In the downlink ISAC scenario, the PAS simultaneously transmit communication and sensing signals to concurrently serve all communication users and perform target detection. The transmitted signal from the base station can be expressed as

$$\mathbf{s} = \mathbf{W}\mathbf{c} + \mathbf{W}_0\mathbf{c}_s \tag{16}$$

where $\mathbf{W} = [\mathbf{w}_1, \mathbf{w}_2, \ldots, \mathbf{w}_{K+L}]$ denotes the beamforming matrix, $\mathbf{w}_k \in \mathbb{C}^{N\times 1}$ represents the beamforming vector allocated to the k-th communication user, $\mathbf{W}_0 \in \mathbb{C}^{N\times 1}$ is the sensing beamforming matrix, and $\mathbf{W}_0\mathbf{c}_s$ denotes the transmitted signal dedicated to the sensing function, where $\mathbf{c}_s \in \mathbb{C}^{N\times 1}$ is the corresponding communication symbol. The communication symbols of different users are mutually independent and satisfy the normalization condition $\mathbb{E}[\mathbf{c}\mathbf{c}^H] = \mathbf{I}_{K+L}$ with $\mathbf{c} = [c_1, c_2, \ldots, c_{K+L}]^T \in \mathbb{C}^{(K+L)\times 1}$.

The signal received by near-field users can be uniformly modeled as

$$y_k = \underbrace{\mathbf{h}_{u,k}^H\mathbf{s}}_{\text{Waveguide feed array signal}} + \underbrace{n_k}_{\text{Receiving end noise}} \tag{17}$$

The signal received by the waveguide located at the receiving position is given by

$$y_m = \underbrace{\mathbf{h}_{r,m}\alpha_m\mathbf{h}_{t,m}^H\mathbf{W}_0\mathbf{c}_s}_{\text{Target echo}} + \underbrace{\mathbf{h}_{r,m}\alpha_m\mathbf{h}_{t,m}^H\mathbf{W}\mathbf{c}}_{\text{Interference of communication signals}} + \underbrace{n_r}_{\text{Receiving end noise}} \tag{18}$$

Here the first term represents the echo reflected from the sensing target carried by the dedicated sensing signal, and the second term denotes the echo component reflected from the target carried by the communication signal. In the ISAC framework, since the communication signal is known at the receiver (BS), it serves as a dual-purpose waveform that contributes to the total sensing energy rather than acting as interference. Furthermore, n_r and n both follow the complex Gaussian distribution $\mathcal{CN}(0, \sigma^2)$ representing the additive white Gaussian noise (AWGN) at the receiver. Additionally, α_m denotes the reflection coefficient of the sensing target.

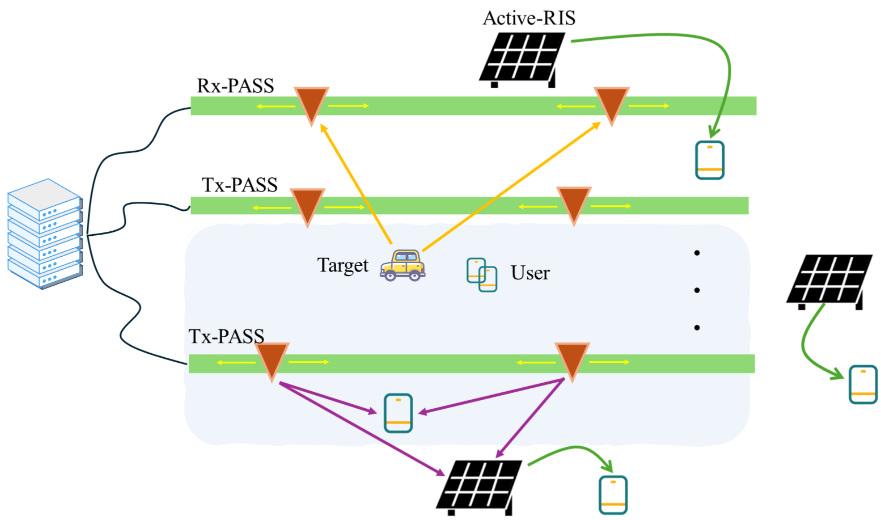

FIGURE 1. System configuration of the reconfigurable antenna system and multi-RIS assisted ISAC downlink network.

Let $\mathbf{h}_l \in \mathbb{C}^{R\times 1}$ denote the channel vector between the l-th RIS and user l. The reflection matrix of the l-th RIS is expressed as

$$\boldsymbol{\Theta}_l = \mathrm{diag}\left(a_{l,1}e^{j\phi^{l,1}}, \ldots, a_{l,R}e^{j\phi^{l,R}}\right) \tag{19}$$

The signal received by user l can be expressed as

$$\begin{aligned} y_l5 = & \underbrace{\mathbf{h}_l^T\boldsymbol{\Theta}_l\tilde{\mathbf{H}}_l^H\mathbf{w}_l c_l}_{\text{effective signal reflected by RIS}} + \sum_{i\neq l}\underbrace{\mathbf{h}_l^T\boldsymbol{\Theta}_l\tilde{\mathbf{H}}_l^H\mathbf{w}_i c_i}_{\substack{\text{signal interference of}\\ \text{communication user interference}}} \\ & + \underbrace{\mathbf{h}_l^T\boldsymbol{\Theta}_l\tilde{\mathbf{H}}_l^H\mathbf{W}_0\mathbf{c}_s}_{\text{perceived signal interference}} \\ & + \underbrace{\mathbf{h}_l^T\boldsymbol{\Theta}_l\mathbf{z}_l}_{\text{RIS thermal noise}} + \underbrace{n_l}_{\text{user-end receives noise}} \end{aligned} \tag{20}$$

where $\mathbf{z}_l \in \mathbb{C}^{R\times 1}$ represents the active thermal noise of the RIS, which follows the distribution $\mathcal{CN}(0, \sigma_{\mathrm{RIS}}^2\mathbf{I}_R)$.

D. SYSTEM PROBLEM MODELING

The received signal-to-noise ratio (SINR) of the perceived target echo at the base station can be defined as

$$\mathrm{SINR}_m = \frac{|\alpha_m|^2\left\|\mathbf{h}_{r,m}\mathbf{h}_{t,m}^H\mathbf{W}_0\right\|^2}{|\alpha_m|^2\left\|\mathbf{h}_{r,m}\mathbf{h}_{t,m}^H\mathbf{W}\right\|^2 + \sigma_r^2} \tag{21}$$

The signal-to-interference-plus-noise ratio (SINR) of the k-th near-field communication user is given by

$$\mathrm{SINR}_k^{\mathrm{near}} = \frac{\left|\mathbf{h}_{u,k}^H\mathbf{w}_k\right|^2}{\sum_{i\neq k}\left|\mathbf{h}_{u,k}^H\mathbf{w}_i\right|^2 + \left\|\mathbf{h}_{u,k}^H\mathbf{W}_0\right\|^2 + \sigma_k^2} \tag{22}$$

The SINR of the l-th far-field communication user is given by

$$\begin{aligned} \mathrm{SINR}_l^{\mathrm{far}} &= \frac{\left|\mathbf{h}_l^T\boldsymbol{\Theta}_l\tilde{\mathbf{H}}_l^H\mathbf{w}_l\right|^2}{\Delta_l^{\mathrm{far}}}, \\ \Delta_l^{\mathrm{far}} &= \sum_{i\neq l}\left|\mathbf{h}_l^T\boldsymbol{\Theta}_l\tilde{\mathbf{H}}_l^H\mathbf{w}_i\right|^2 \\ &\quad + \left\|\mathbf{h}_l^T\boldsymbol{\Theta}_l\tilde{\mathbf{H}}_l^H\mathbf{W}_0\right\|^2 + \sigma_{\mathrm{RIS}}^2\left\|\mathbf{h}_l^T\boldsymbol{\Theta}_l\right\|^2 + \sigma_l^2 \end{aligned} \tag{23}$$

The corresponding sum rates of the near-field communication users and far-field users can be defined as

$$Q_{\mathrm{near}} = \sum_{c=1}^{K}\log_2\left(1 + \mathrm{SINR}_c^{\mathrm{near}}\right) \tag{24}$$

$$Q_{\mathrm{far}} = \sum_{l=1}^{L}\log_2\left(1 + \mathrm{SINR}_l^{\mathrm{far}}\right) \tag{25}$$

The total power consumption of the system can be expressed as

$$\begin{aligned} P_{\mathrm{total}} = & \xi\mathrm{Tr}\left(\mathbf{W}_0\mathbf{W}_0^H + \mathbf{W}\mathbf{W}^H\right) + \xi_{\mathrm{RIS},l}P_{\mathrm{RIS},l} \\ & + P_{\mathrm{fix}} + P_{\mathrm{move}}\left(\mathbf{X}, \mathbf{X}_r\right) \end{aligned} \tag{26}$$

where ξ denotes the power amplifier efficiency of the base station. $\mathrm{Tr}(\mathbf{W}_0\mathbf{W}_0^H + \mathbf{W}\mathbf{W}^H)$ represents the total power transmitted by the base station for communication and sensing signals, which constitutes the most significant variable power term in energy efficiency optimization. The term $P_{\text{move}}(\mathbf{X}, \mathbf{X}_r)$ represents the dynamic power consumption required for the mechanical repositioning of the pinching antennas along the waveguides. In industrial textile environments, this component is non-negligible and depends on the displacement of the antennas during the optimization process.

The power consumption of the RIS comprises three components: the static circuit power of each reflecting element $P_c(R)$, the DC biasing power P_{DC}, and the power consumption of the active RIS amplifier $\xi_{\text{RIS},a} P_{\text{out}}(\boldsymbol{\Theta})$. The output power of the l-th RIS can be expressed as

$$P_{\text{out}}(\boldsymbol{\Theta}_l) = \left\| \boldsymbol{\Theta}_l \tilde{\mathbf{H}}_l^H \mathbf{W} \right\|^2 + \left\| \boldsymbol{\Theta}_l \tilde{\mathbf{H}}_l^H \mathbf{W}_0 \right\|^2 + \sigma_l^2 \left\| \boldsymbol{\Theta}_l \right\|^2 \tag{27}$$

Furthermore, the fixed power consumption term P_{fix} encompasses the static circuit power of the base station, the hardware power consumption of each user terminal, the biasing and driving power of the PAS, as well as the control and tuning circuit power, among others. Since these components are independent of the optimization variables, they are typically treated as constants in energy efficiency analysis [13]. Unlike traditional models that treat all non-RF power as a constant, this study acknowledges the mechanical energy requirements of PASS as a significant variable in the energy efficiency analysis, ensuring a more realistic evaluation of the system's performance in automated production lines.

The energy efficiency (EE) of the communication user is then defined as

$$\text{EE} = \frac{Q_{\text{near}} + Q_{\text{far}}}{P_{\text{total}}} \tag{28}$$

In this work, our objective is to maximize the sum energy efficiency. While the objective function treats Q_{near} and Q_{far} as a sum, their underlying channel models and power dependencies are distinct. Specifically, the optimization of Q_{far} is tightly coupled with the active RIS reflection matrix $\boldsymbol{\Theta}$, whereas Q_{near} is predominantly influenced by the PASS antenna deployment $\mathbf{X}$. This mathematical separation in the constraints and channel vectors ensures that the unique physical requirements of each region are preserved during the joint optimization process. Accordingly, the problem can be formulated as

$$\max_{\mathbf{W}, \mathbf{W}_0, \{\boldsymbol{\Theta}_l\}_{l=1}^L, \mathbf{X}, \mathbf{X}_r} \quad \text{EE} \tag{29a}$$

$$\text{s.t.} \quad \text{SINR}_m \geq \gamma, \tag{29b}$$

$$\xi \text{Tr}\left(\mathbf{W}_0 \mathbf{W}_0^H + \mathbf{W}\mathbf{W}^H\right) \leq P_{\text{BS}}, \tag{29c}$$

$$P_{\text{RIS},l} \leq P_g, \quad \forall l = 1, \ldots, L \tag{29d}$$

$$|a_{l,r}| \leq a_{\max}, \quad l = 1, \ldots, L, \; r = 1, \ldots, R \tag{29e}$$

$$[\mathbf{X}]_{n,m} \in \mathcal{X}, \quad n = 1, \ldots, N, \quad m = 1, \ldots, M \tag{29f}$$

$$[\mathbf{X}_r]_{n,m} \in \mathcal{X}_r, \quad n = 1, \ldots, N, \quad m = 1, \ldots, M \tag{29g}$$

Here (29b) represents the threshold constraint on the received sensing echo. Constraints (29c) and (29d) impose the power limitations on the base station and each active RIS, respectively. Constraint (29e) characterizes the physical constraints of the active RIS reflecting elements. Constraints (29f) and (29g) specify the deployment position constraints for each pinching antenna on the receive and transmit waveguides, respectively.

III. PROBLEM-SOLVING

To solve the original optimization problem containing non-convex coupling terms, the alternating optimization (AO) framework is employed to decompose the problem into multiple subproblems, which are then updated iteratively. To address the non-convexity introduced by the logarithmic terms and fractional structure in (29a), the fractional programming (FP) method from [14] is adopted to perform equivalent transformations on the relevant terms, thereby decoupling the coupled variables and enabling the separate optimization of each variable within the AO framework.

Within the Dinkelbach iterative framework, the parameter μ is updated at each iteration according to the following rule:

$$\mu^{(t+1)} = \frac{Q_{\text{near}} + Q_{\text{far}}}{P_{\text{total}}}$$

After fixing the auxiliary variable μ, the objective function in (30) still contains logarithmic terms and a fractional structure, rendering the overall problem non-convex.

$$\max_{\mathbf{W}, \mathbf{W}_0, \{\boldsymbol{\Theta}_l\}, \mathbf{X}, \mathbf{X}_r} Q_{\text{near}} + Q_{\text{far}} - \mu P_{\text{total}} \tag{30}$$

To further separate the numerator and denominator in the SINR expressions and transform the logarithmic-form rate function into a more tractable structure, two sets of auxiliary variables $\rho = \{\rho_k^{\text{near}}, \rho_i^{\text{far}}\}$ and $\nu = \{\nu_k^{\text{near}}, \nu_i^{\text{far}}\}$ are introduced to eliminate the coupling in the logarithmic and fractional terms, respectively. Based on these variables, the equivalent reformulation can be expressed as

$$f\left(W,W_0,\Theta,\rho,\upsilon,X,X_r\right)=g\left(W,W_0,\Theta,\rho,\upsilon,X,X_r\right)-\mu P_{\text{total}} \tag{31}$$

where $g\left(W,W_0,\Theta,\rho,\upsilon,X,X_r\right)$

$$\begin{aligned}
&=\sum_{k=1}^{K}\Bigg[\ln(1+\rho_k^{\text{near}})-\rho_k^{\text{near}}+2\sqrt{1+\rho_k^{\text{near}}}\Re\{(\nu_k^{\text{near}})^*\mathbf{h}_{u,k}^H\mathbf{w}_k\}\\
&\quad-|\nu_k^{\text{near}}|^2\left(\sum_{k'=1}^{K}|\mathbf{h}_{u,k}^H\mathbf{w}_{k'}|^2+\|\mathbf{h}_{u,k}^H\mathbf{W}_0\|^2+\sigma_0^2\right)\Bigg]\\
&+\sum_{i=1}^{L}\Bigg[\ln(1+\rho_i^{\text{far}})-\rho_i^{\text{far}}+2\sqrt{1+\rho_i^{\text{far}}}\Re\{(\nu_i^{\text{far}})^*\mathbf{h}_i^H\mathbf{\Theta}_i\tilde{\mathbf{H}}_i\mathbf{w}_i\}\\
&\quad-|\nu_i^{\text{far}}|^2\left(\sum_{k'=1}^{K}|\mathbf{h}_i^H\mathbf{\Theta}_i\tilde{\mathbf{H}}_i\mathbf{w}_{k'}|^2+\sigma_0^2\right)\\
&\quad-|\nu_i^{\text{far}}|^2\left(\|\mathbf{h}_i^H\mathbf{\Theta}_i\tilde{\mathbf{H}}_i\mathbf{W}_0\|^2+\|\mathbf{h}_i^H\mathbf{\Theta}_i\|^2\sigma_{\text{RIS}}^2\right)\Bigg]
\end{aligned} \tag{32}$$

Equation (32) presents the equivalent rate formulation obtained after applying the quadratic transform and Lagrangian dual transform, where the numerator-denominator coupling in both the near-field and far-field communication terms has been eliminated. For given $(\mathbf{W},\mathbf{W}_0,\mathbf{\Theta})$, the optimization with respect to the auxiliary variables ρ and ν constitutes unconstrained problems, whose optimal solutions can be obtained by setting the partial derivatives to zero, i.e., $\frac{\partial f}{\partial \rho}=0$, $\frac{\partial f}{\partial \nu}=0$. According to the derivation, we obtain:

$$\rho_k^{(\cdot)}=\frac{\iota_k^{(\cdot)}}{2}\left(\iota_k^{(\cdot)}+\sqrt{(\iota_k^{(\cdot)})^2+4}\right) \tag{33}$$

$$\nu_k^{\text{near}}=\frac{\sqrt{1+\rho_k^{\text{near}}}\mathbf{h}_{u,k}^H\mathbf{w}_{u,k}}{\sum_{i=1}^{K}|\mathbf{h}_{u,k}^H\mathbf{w}_i|^2+\|\mathbf{h}_{u,k}^H\mathbf{W}_0\|^2+\sigma_k^2} \tag{34}$$

$$\nu_k^{\text{far}}=\frac{\sqrt{1+\rho_k^{\text{far}}}\mathbf{h}_k^H\mathbf{\Theta}_k\tilde{\mathbf{H}}_k\mathbf{w}_k}{\|\mathbf{h}_k^H\mathbf{\Theta}_k\tilde{\mathbf{H}}_k\mathbf{W}_0\|^2+\|\mathbf{h}_k^H\mathbf{\Theta}_k\|^2\sigma_{\text{RIS}}^2+\sum_{k'=1}^{K}|\mathbf{h}_k^H\mathbf{\Theta}_k\tilde{\mathbf{H}}_k\mathbf{w}_{k'}|^2+\sigma_0^2}. \tag{35}$$

where $(\cdot)\in\{\text{near},\text{far}\}$, and

$$\iota_k^{\text{near}}=\Re\left\{(\nu_k^{\text{near}})^*\mathbf{h}_{u,k}^H\mathbf{w}_k\right\} \tag{36}$$

$$\iota_k^{\text{far}}=\Re\left\{(\nu_k^{\text{far}})^*\mathbf{h}_k^H\mathbf{\Theta}_k\tilde{\mathbf{H}}_k\mathbf{w}_k\right\} \tag{37}$$

Upon obtaining the closed-form solutions for the auxiliary variables $(\rho^\star,\nu^\star)$, the objective function can be further simplified to the following equivalent form:

$$\max_{\mathbf{W},\mathbf{W}_0,\mathbf{\Theta},\mathbf{X},\mathbf{X}_r} f(\mathbf{W},\mathbf{W}_0,\mathbf{\Theta},\mathbf{X},\mathbf{X}_r)\quad \text{s.t. } (25b)-(25g). \tag{38}$$

At this point, the original energy efficiency maximization problem has been transformed into an equivalent optimization formulation with respect to $\mu,\rho,\nu,\mathbf{W},\mathbf{W}_0,\mathbf{\Theta}$, which can be iteratively solved to achieve convergence through alternating updates of each set of variables.

A. OPTIMIZATION OF BEAMFORMING

With $(\mathbf{X},\mathbf{X}_r,\mathbf{\Theta})$ fixed, the beamforming optimization subproblem can be reformulated as the following equivalent form, where the relevant auxiliary vectors and matrices are defined as follows:

$$\begin{aligned}
\bar{\mathbf{w}}_0&=[\mathbf{w}_{0,1}^T,\ldots,\mathbf{w}_{0,N}^T]^T,\\
\bar{\mathbf{w}}_{\text{near}}&=[\mathbf{w}_1^T,\ldots,\mathbf{w}_K^T]^T,\\
\bar{\mathbf{w}}_{\text{far}}&=[\mathbf{w}_{K+1}^T,\ldots,\mathbf{w}_{K+L}^T]^T,\\
\mathbf{b}_{\text{near},k}^H&=2\sqrt{1+\rho_k^{\text{near}}}(\nu_k^{\text{near}})^*\mathbf{h}_{u,k}^H,\\
\mathbf{b}_{\text{far},k}^H&=2\sqrt{1+\rho_k^{\text{far}}}(\nu_k^{\text{far}})^*\mathbf{h}_k^H\mathbf{\Theta}_k\tilde{\mathbf{H}}_k^H,\\
\mathbf{B}_{\text{near}}&=[\mathbf{b}_{\text{near},1}^H,\ldots,\mathbf{b}_{\text{near},K}^H],\\
\mathbf{B}_{\text{far}}&=[\mathbf{b}_{\text{far},K+1}^H,\ldots,\mathbf{b}_{\text{far},K+L}^H],\\
\mathbf{A}_{\text{near}}&=\mathbf{I}_{K+L}\otimes\left(\sum_{k=1}^{K}|\nu_{\text{near},k}|^2\mathbf{h}_{u,k}\mathbf{h}_{u,k}^H\right),\\
\mathbf{A}_{\text{far}}&=\mathbf{I}_{K+L}\otimes\left[\sum_{k=K+1}^{K+L}|\nu_{\text{far},k}|^2(\mathbf{h}_k\mathbf{\Theta}_k\tilde{\mathbf{H}}_k^H)^H(\mathbf{h}_k\mathbf{\Theta}_k\tilde{\mathbf{H}}_k^H)\right],\\
\mathbf{C}_{\text{near}}&=\mathbf{I}_N\otimes\left(\sum_{k=1}^{K}|\nu_{\text{near},k}|^2\mathbf{h}_{u,k}\mathbf{h}_{u,k}^H\right),\\
\mathbf{C}_{\text{far}}&=\mathbf{I}_N\otimes\left[\sum_{k=K+1}^{K+L}|\nu_{\text{far},k}|^2(\mathbf{h}_k\mathbf{\Theta}_k\tilde{\mathbf{H}}_k^H)^H(\mathbf{h}_k\mathbf{\Theta}_k\tilde{\mathbf{H}}_k^H)\right],\\
\mathbf{D}&=\mathbf{I}_{K+L}\otimes\left(\sum_{r=1}^{L}(\mathbf{\Theta}_r\tilde{\mathbf{H}}_r^H)^H(\mathbf{\Theta}_r\tilde{\mathbf{H}}_r^H)\right),\\
\tilde{\mathbf{D}}&=\mathbf{I}_N\otimes\left(\sum_{r=1}^{L}(\mathbf{\Theta}_r\tilde{\mathbf{H}}_r^H)^H(\mathbf{\Theta}_r\tilde{\mathbf{H}}_r^H)\right),\\
\mathbf{S}&=\mathbf{I}_{K+L}\otimes\left((\mathbf{\Theta}_r\tilde{\mathbf{H}}_r^H)^H(\mathbf{\Theta}_r\tilde{\mathbf{H}}_r^H)\right),\\
\tilde{\mathbf{S}}&=\mathbf{I}_N\otimes\left((\mathbf{\Theta}_r\tilde{\mathbf{H}}_r^H)^H(\mathbf{\Theta}_r\tilde{\mathbf{H}}_r^H)\right).
\end{aligned}$$

Based on the above variable definitions, the objective function can be further equivalently reformulated as

$$\begin{aligned}
\max_{\bar{\mathbf{w}}_{\text{near}},\bar{\mathbf{w}}_{\text{far}},\bar{\mathbf{w}}_0}\ &\Re\{\mathbf{B}_{\text{near}}^H\bar{\mathbf{w}}_{\text{near}}+\mathbf{B}_{\text{far}}^H\bar{\mathbf{w}}_{\text{far}}\}\\
&-\bar{\mathbf{w}}^H(\mathbf{A}_{\text{near}}+\mathbf{A}_{\text{far}})\bar{\mathbf{w}}-\bar{\mathbf{w}}_0^H(\mathbf{C}_{\text{near}}+\mathbf{C}_{\text{far}})\bar{\mathbf{w}}_0\\
&-\mu\bar{\mathbf{w}}^H\mathbf{D}\bar{\mathbf{w}}-\mu\bar{\mathbf{w}}_0^H\tilde{\mathbf{D}}\bar{\mathbf{w}}_0-\mu\bar{\mathbf{w}}_0^H\bar{\mathbf{w}}_0-\mu\bar{\mathbf{w}}^H\bar{\mathbf{w}},
\end{aligned} \tag{39}$$

where $\bar{\mathbf{w}}=[\bar{\mathbf{w}}_{\text{near}}^T,\bar{\mathbf{w}}_{\text{far}}^T]^T$ is defined. The active-RIS and base-station power constraints can be written as

$$\bar{\mathbf{w}}^H\mathbf{S}\bar{\mathbf{w}}+\bar{\mathbf{w}}_0^H\tilde{\mathbf{S}}\bar{\mathbf{w}}_0+\sigma_l^2\|\mathbf{\Theta}_r\|^2\le P_{\text{PA}}, \tag{40}$$

$$\bar{\mathbf{w}}^H\bar{\mathbf{w}}+\bar{\mathbf{w}}_0^H\bar{\mathbf{w}}_0\le P_{\text{BS}}. \tag{41}$$

where $\bar{\mathbf{w}}=[\hat{\mathbf{w}}_{\text{near}},\hat{\mathbf{w}}_{\text{far}}]$ is defined. To handle the non-convex term in constraint (29b), an identity transformation is first employed to equivalently reformulate it, yielding the following separated form:

$$\begin{aligned}
&|\alpha_m|^2\left\|\mathbf{h}_{r,m}\mathbf{h}_{t,m}^H\mathbf{W}_0\right\|^2\\
&-\gamma\left(|\alpha_m|^2\left\|\mathbf{h}_{r,m}\mathbf{h}_{t,m}^H\mathbf{W}\right\|^2+\sigma_r^2\right)\ge 0
\end{aligned} \tag{42}$$

Subsequently, by applying a first-order Taylor expansion at the current iteration point $\widetilde{\mathbf{W}}_0$ to convexify the first term with respect to $\mathbf{W}_0$, the non-convex constraint (29b) can be transformed into the following tractable form:

$$|\alpha_m|^2 \widetilde{\mathbf{w}}_0^H \widetilde{\mathbf{D}} \widetilde{\mathbf{w}}_0 - \gamma |\alpha_m|^2 \bar{\mathbf{w}}^H \widetilde{\mathbf{D}} \bar{\mathbf{w}} - \gamma \sigma_r^2 + 2|\alpha_m|^2 \Re\left\{ \widetilde{\mathbf{w}}_0^H \widetilde{\mathbf{D}} (\mathbf{w}_0 - \widetilde{\mathbf{w}}_0) \right\} \tag{43}$$

Based on the above transformation, the original problem is transformed into maximizing (39) subject to (40), (41), and (43).

B. OPTIMIZATION OF ACTIVE RIS REFLECTION MATRIX

With $(\mathcal{X}, \mathcal{X}_r, \mathbf{W}, \mathbf{W}_0)$ fixed, the optimization variable is reduced to the active RIS reflection matrix $\mathbf{\Theta}$ only. For ease of manipulation, we define $\mathbf{\Phi}_l = [p_{l,1} e^{j\theta_{l,1}}, \ldots, p_{l,R} e^{j\theta_{l,R}}]^H$. Through the identity transformation $\mathrm{diag}(\mathbf{\Phi}_i^H) = \mathbf{\Theta}_i$, the equivalent channel from the RIS to user l can be rewritten as

$$\mathbf{h}_i^H = \mathbf{h}_i^H \mathbf{\Theta}_i \tilde{\mathbf{H}}_i = \mathbf{\Phi}_i^H \mathrm{diag}(\mathbf{h}_i^H) \tilde{\mathbf{H}}_i$$

Based on this, the following auxiliary matrices are introduced:

$$\begin{aligned}
\mathbf{E}_i &= 2\sqrt{1+\rho_i^{\mathrm{far}}} \nu_i^{\mathrm{far}*} \mathrm{diag}(\mathbf{h}_i^H) \tilde{\mathbf{H}}_i \mathbf{w}_i, \\
\mathbf{F}_i &= \sum_{k=1}^{K} |\nu_i^{\mathrm{far}*}|^2 \mathrm{diag}(\mathbf{h}_i^H) \tilde{\mathbf{H}}_i \mathbf{w}_k \mathbf{w}_k^H \tilde{\mathbf{H}}_i^H \mathrm{diag}(\mathbf{h}_i), \\
\mathbf{G}_i &= \sum_{k=1}^{K} |\nu_i^{\mathrm{far}*}|^2 \mathrm{diag}(\mathbf{h}_i^H) \tilde{\mathbf{H}}_i \mathbf{w}_k \mathbf{w}_k^H \tilde{\mathbf{H}}_i^H \mathrm{diag}(\mathbf{h}_i), \\
\mathbf{J}_i &= \sum_{k=1}^{N} |\nu_i^{\mathrm{far}*}|^2 \mathrm{diag}(\mathbf{h}_i^H) \mathrm{diag}(\mathbf{h}_i), \\
\mathbf{O}_i &= \sum_{k=1}^{K+L} \mathrm{diag}(\tilde{\mathbf{H}}_i^H \mathbf{w}_k) \mathrm{diag}(\tilde{\mathbf{H}}_i^H \mathbf{w}_k)^H + \sigma_i^2 \mathbf{I}_R.
\end{aligned}$$

According to the above definition, the active RIS optimization sub-problem can be equivalently written as

$$\max_{\{\mathbf{\Phi}_i\}_{i=1}^{L}} \sum_{i=1}^{L} \mathbf{\Phi}_i^H \mathbf{E}_i - \mathbf{\Phi}_i^H (\mathbf{F}_i + \mathbf{G}_i + \mathbf{J}_i) \mathbf{\Phi}_i - \sum_{i=1}^{L} \mu \mathbf{\Phi}_i^H \mathbf{O}_i \mathbf{\Phi}_i, \tag{44}$$

$$\mathbf{\Phi}_i^H \mathbf{O}_i \mathbf{\Phi}_i \leq P_{\mathrm{PA}}, \quad i = 1, \ldots, L, \tag{45}$$

$$P_{l,R} \leq a_{\max}, \quad r = 1, \ldots, R, \; i = 1, \ldots, L. \tag{46}$$

C. OPTIMIZATION OF PASS ANTENNA POSITIONS

With $(\mathbf{W}, \mathbf{W}_0, \mathbf{\Theta})$ fixed, the optimization is performed with respect to $\mathbf{X}$ and $\mathbf{X}_r$. First, the equivalent channel matrix between the m-th antenna on all transmit waveguides and the sensing target is expressed as

$$\mathbf{h}_{t,m} = \sum_{m=1}^{M} \tilde{\mathbf{h}}_{t,m} \in \mathbb{C}^{N \times 1}, \tag{47}$$

where $\tilde{\mathbf{h}}_{t,m}$ represents the subchannel contribution of the m-th pinching antenna across all waveguides to the sensing target. Furthermore, the equivalent channel between the PASS and all RIS is expressed as

$$\tilde{\mathbf{H}}_i = [\tilde{\mathbf{H}}_{i,1}, \tilde{\mathbf{H}}_{i,2}, \ldots, \tilde{\mathbf{H}}_{i,L}] = \sum_{m=1}^{M} \tilde{\mathbf{H}}_{i,m} \in \mathbb{C}^{N \times RL} \tag{48}$$

For the m-th antenna on the waveguide, the corresponding auxiliary matrices $\mathbf{q}_m$ and $\mathbf{Q}_m$ are defined, and $\mathbf{Q}_m$ is partitioned according to the m-th antenna across all waveguides to each RIS as follows:

$$\mathbf{Q}_m = [\mathbf{Q}_{1,m}, \mathbf{Q}_{2,m}, \ldots, \mathbf{Q}_{L,m}], \quad \forall m = 1, \ldots, M \tag{49}$$

The auxiliary channel vector from the PASS to the l-th RIS is denoted as

$$\mathbf{Q}_{u,l} = \sum_{m=1}^{M} \mathbf{Q}_{l,m}, \quad l = 1, 2, \ldots, L. \tag{50}$$

Based on the above definitions, the transmit auxiliary matrix for the PASS-sensing target link, as well as the overall auxiliary matrix from the PASS to all RIS, can be obtained as

$$\mathbf{q}_{s,T} = \sum_{m=1}^{M} \mathbf{q}_m \in \mathbb{C}^{N \times 1}, \tag{51}$$

$$\mathbf{Q} = [\mathbf{Q}_{u,1}, \mathbf{Q}_{u,2}, \ldots, \mathbf{Q}_{u,L}] = \sum_{m=1}^{M} \mathbf{Q}_m \in \mathbb{C}^{N \times RM} \tag{52}$$

Similarly, the link from the m-th antenna on the receive waveguide to the sensing target is denoted as $\tilde{\mathbf{h}}_{r,m}$, and its corresponding receive auxiliary vector is defined as $\mathbf{q}_r = \sum_{m=1}^{M} \mathbf{q}_{r,m}$. On this basis, the original optimization problem can be restated as the following constrained formula:

$$\max_{\mathbf{X}, \mathbf{X}_r, \mathbf{q}, \mathbf{Q}, \tilde{\mathbf{q}}} f(\mathbf{W}, \mathbf{W}_0, \mathbf{\Theta}, \mathbf{X}, \mathbf{X}_r), \tag{53}$$

$$\text{s.t.} \quad \mathbf{q}_m = \tilde{\mathbf{h}}_{t,m}, \quad \mathbf{q}_{s,T} = \sum_{m=1}^{M} \mathbf{q}_m, \quad m \in \mathcal{M}, \tag{54}$$

$$\mathbf{Q}_m = \tilde{\mathbf{H}}_{i,m}, \quad \mathbf{Q} = \sum_{m=1}^{M} \mathbf{Q}_m, \quad \forall m \in \mathcal{M}, \tag{55}$$

$$\mathbf{q}_{r,m} = \tilde{\mathbf{h}}_{r,m}, \quad \mathbf{q}_r = \sum_{m=1}^{M} \mathbf{q}_{r,m}, \quad m \in \mathcal{M} \tag{56}$$

$$\frac{|\alpha_k|^2 \|\mathbf{q}_r \mathbf{q}_{s,T} \mathbf{W}_0\|^2}{|\alpha_k|^2 \|\mathbf{q}_r \mathbf{q}_{s,T} \mathbf{W}\|^2 + \sigma_k^2} \geq \tau, \tag{57}$$

$$\|\mathbf{\Theta}_l \mathbf{Q}_{u,l} \mathbf{W}\|^2 + \|\mathbf{\Theta}_l \mathbf{Q}_{u,l} \mathbf{W}_0\|^2 + \sigma_l^2 \|\mathbf{\Theta}_l\|^2 \leq P_{\mathrm{A}}, \tag{58}$$

$$[\mathbf{X}]_{n,m} \in \mathcal{X}, \quad [\mathbf{X}_r]_{n,m} \in \mathcal{X}_r. \tag{59}$$

Subsequently, by introducing consistency constraints through the penalty function method, the above problem is further relaxed as

$$\max_{\substack{\mathbf{X},\mathbf{Q},\{\mathbf{Q}_m\}_{m=1}^M\\ \mathbf{q}_{s,T},\{\mathbf{q}_m\}_{m=1}^M\\ \tilde{\mathbf{q}},\{\mathbf{q}_{r,m}\}_{m=1}^M}} (50)-\frac{1}{\rho_1}\left\|\mathbf{Q}-\sum_{m=1}^M\mathbf{Q}_m\right\|_F^2-\frac{1}{\rho_3}\sum_{m=1}^M\|\mathbf{q}_{r,m}-\tilde{\mathbf{h}}_{r,m}\|^2$$
$$-\frac{1}{\rho_1}\sum_{m=1}^M\|\mathbf{Q}_m-\tilde{\mathbf{H}}_{i,m}\|_F^2-\frac{1}{\rho_2}\left\|\mathbf{q}_{s,T}-\sum_{m=1}^M\mathbf{q}_m\right\|_F^2$$
$$-\frac{1}{\rho_2}\sum_{m=1}^M\|\mathbf{q}_m-\tilde{\mathbf{h}}_{t,m}\|_F^2-\frac{1}{\rho_1}\left\|\mathbf{q}_r-\sum_{m=1}^M\mathbf{q}_{r,m}\right\|_F^2. \quad (60)$$

1) Update of Auxiliary Channel Matrix Variables

With $(\mathbf{X},\mathbf{X}_r,\mathbf{Q}_m,\mathbf{q}_m,\mathbf{q}_{r,m})$ fixed, the optimization is performed with respect to $\mathbf{Q}$, $\tilde{\mathbf{q}}_r$, and $\mathbf{q}_{s,T}$.

$$\min_{\mathbf{Q},\mathbf{q}_{s,T},\tilde{\mathbf{q}}_r} \quad -\frac{1}{\rho_1}\left\|\mathbf{Q}-\sum_{m=1}^M\mathbf{Q}_m\right\|_F^2+\frac{1}{\rho_2}\left\|\mathbf{q}_{s,T}-\sum_{m=1}^M\mathbf{q}_m\right\|_F^2$$
$$+\frac{1}{\rho_3}\left\|\mathbf{q}_r-\sum_{m=1}^M\mathbf{q}_{r,m}\right\|_F^2 \quad (61)$$

s.t. (57), (58), where (61) and (58) are convex functions with respect to $\mathbf{Q}$, $\tilde{\mathbf{q}}_r$, $\mathbf{q}_{s,T}$, while (57) constitutes a non-convex constraint containing coupling terms, which can be expressed as:

$$\frac{|\alpha_k|^2}{\tau}\|\mathbf{q}_r\mathbf{q}_{s,T}\mathbf{W}_0\|^2-|\alpha_k|^2\|\mathbf{q}_r\mathbf{q}_{s,T}\mathbf{W}\|^2+\sigma_k^2. \quad (62)$$

The coupling term $\|\mathbf{q}_r\mathbf{q}_{s,T}\mathbf{W}\|^2$ in this constraint simultaneously depends on both the receive-side variable $\tilde{\mathbf{q}}_r$ and the transmit-side variable $\mathbf{q}_{s,T}$, rendering the subproblem non-convex. To address this, we employ a first-order Taylor approximation to convexify this term. With $\tilde{\mathbf{q}}_r$ fixed, the non-convex term $-|\alpha_k|^2\|\mathbf{q}_r\mathbf{q}_{t,m}\mathbf{W}\|^2$ can be expanded at the point $\mathbf{q}_{s,T}^{(t)}$ as follows:

$$-|\alpha_k|^2\left\|\mathbf{q}_r\mathbf{q}_{s,T}^{(t)}\mathbf{W}\right\|^2$$
$$+2\Re\left\{\left[-2|\alpha_k|^2\mathbf{q}_r^H\mathbf{q}_r\mathbf{q}_{s,T}^{(t)}\mathbf{W}\mathbf{W}^H\right]^H\left(\mathbf{q}_{s,T}-\mathbf{q}_{s,T}^{(t)}\right)\right\}. \quad (63)$$

Thus, the constraint (57) can be convex approximated as:

$$\frac{|\alpha_k|^2}{\tau}\|\mathbf{q}_r\mathbf{q}_{s,T}\mathbf{W}_0\|^2-|\alpha_k|^2\left\|\mathbf{q}_r\mathbf{q}_{s,T}^{(t)}\mathbf{W}\right\|^2$$
$$+2\Re\left\{\left[-2|\alpha_k|^2\mathbf{q}_r^H\mathbf{q}_r\mathbf{q}_{s,T}^{(t)}\mathbf{W}\mathbf{W}^H\right]^H\left(\mathbf{q}_{s,T}-\mathbf{q}_{s,T}^{(t)}\right)\right\}. \quad (64)$$

From the above content, the following convex constraint problems can be obtained:

$$\min_{\mathbf{Q},\mathbf{q}_{s,T},\tilde{\mathbf{q}}_r} \quad -\frac{1}{\rho_1}\left\|\mathbf{Q}-\sum_{m=1}^M\mathbf{Q}_m\right\|_F^2+\frac{1}{\rho_2}\left\|\mathbf{q}_{s,T}-\sum_{m=1}^M\mathbf{q}_m\right\|_F^2$$
$$+\frac{1}{\rho_3}\left\|\mathbf{q}_r-\sum_{m=1}^M\mathbf{q}_{r,m}\right\|_F^2 \quad (65)$$

s.t. (58), (64).

2) Update of Per-Antenna Auxiliary Vectors

With $(\mathbf{X},\mathbf{X}_r,\mathbf{Q},\mathbf{q}_{s,T},\mathbf{q}_r)$ fixed, the updates are performed for $\mathbf{Q}_m$, $\mathbf{q}_m$, and $\mathbf{q}_{r,m}$. This step corresponds to the following optimization problem:

$$\min_{\mathbf{Q}_m,\mathbf{q}_m,\tilde{\mathbf{q}}_{r,m}} \quad \frac{1}{\rho_1}\left\|\mathbf{Q}-\sum_{m=1}^M\mathbf{Q}_m\right\|_F^2$$
$$+\frac{1}{\rho_3}\sum_{m=1}^M\|\mathbf{q}_{r,m}-\tilde{\mathbf{h}}_{r,m}\|^2+\frac{1}{\rho_1}\sum_{m=1}^M\|\mathbf{Q}_m-\tilde{\mathbf{H}}_{i,m}\|_F^2$$
$$+\frac{1}{\rho_2}\left\|\mathbf{q}_{s,T}-\sum_{m=1}^M\mathbf{q}_m\right\|_F^2+\frac{1}{\rho_2}\sum_{m=1}^M\|\mathbf{q}_m-\tilde{\mathbf{h}}_{t,m}\|_F^2$$
$$+\frac{1}{\rho_3}\left\|\mathbf{q}_r-\sum_{m=1}^M\mathbf{q}_{r,m}\right\|_F^2. \quad (66)$$

This problem is an unconstrained convex quadratic optimization problem. Considering the optimization of $\mathbf{Q}_m$, the objective function is denoted as

$$f(\mathbf{Q}_1,\ldots,\mathbf{Q}_M)=\frac{1}{\rho_1}\left\|\mathbf{Q}-\sum_{m=1}^M\mathbf{Q}_m\right\|_F^2+\frac{1}{\rho_1}\sum_{m=1}^M\left\|\mathbf{Q}_m-\tilde{\mathbf{H}}_{i,m}\right\|_F^2. \quad (67)$$

By setting the gradient of f with respect to any $\mathbf{Q}_m$ to zero, the first-order optimality conditions can be obtained:

$$\mathbf{Q}-\sum_{m=1}^M\mathbf{Q}_m=\mathbf{Q}_m-\mathbf{H}_{l,m}. \quad (68)$$

Summing both sides over m yields

$$M\left(\mathbf{Q}-\sum_{m=1}^M\mathbf{Q}_m\right)=\sum_{m=1}^M(\mathbf{Q}_m-\mathbf{H}_{l,m}). \quad (69)$$

Let $\mathbf{S}=\sum_{m=1}^M\mathbf{Q}_m$; then the above equation can be written as

$$M(\mathbf{Q}-\mathbf{S})=\mathbf{S}-\sum_{m=1}^M\mathbf{H}_{l,m}. \quad (70)$$

Substituting this result into the first-order condition of $\mathbf{Q}_m$, the closed-form optimal solution can be obtained as

$$\mathbf{Q}_m^\star=\mathbf{H}_{l,m}+\frac{1}{M+1}\left(\mathbf{Q}-\sum_{i=1}^M\mathbf{H}_{l,i}\right). \quad (71)$$

Similarly, the closed-form solutions for $\mathbf{q}_m$ and $q_{r,m}$ are given by

$$q_m^\star = \frac{1}{M+1}\left(q_{s,T} - \sum_{m'=1}^{M}\tilde{h}_{t,m'}\right) + \tilde{h}_{t,m} \tag{72}$$

$$q_{r,m}^\star = \frac{1}{M+1}\left(\overline{q}_r - \sum_{m'=1}^{M}\tilde{h}_{r,m'}\right) + \tilde{h}_{r,m} \tag{73}$$

3) Update of the Transmit Antenna Position Variable $\mathbf{X}$

With $\mathbf{Q}$, ${\boldsymbol{Q}_m}_{m=1}^M$ and $\boldsymbol{q}_{s,T}$, $\mathbf{q}_m$ fixed, the subproblem with respect to the position variable $\mathbf{X}$ can be formulated as

$$\max f(\boldsymbol{W},\boldsymbol{W}_0,\boldsymbol{X},\boldsymbol{X}_r) - \frac{1}{\rho_1}\sum_{m=1}^{M}\|\boldsymbol{Q}_m - \tilde{\boldsymbol{H}}_{i,m}\|_F^2 - \frac{1}{\rho_2}\sum_{m=1}^{M}\|\boldsymbol{q}_m - \tilde{\boldsymbol{h}}_{t,m}\|_F^2 \tag{74}$$

$$\text{s.t.} \quad [\mathbf{X}]_{n,m} \in \mathcal{X}. \tag{75}$$

The optimization variables in (74) and (75) appear simultaneously in both the objective function and the constraint terms, resulting in a strongly coupled update structure. To reduce the computational complexity, this section adopts a per-element update strategy: in each iteration, only the position of the m-th movable antenna on the waveguide is optimized while the remaining positions are held fixed. Since the positions of all other antennas are fixed, the feasible region of the m-th antenna can be confined to a deterministic interval, thereby transforming the original high-dimensional coupled problem into an independent optimization of a one-dimensional position variable. The corresponding optimization subproblem can be formulated as

$$\max_{X_m^n} f(\boldsymbol{W},\boldsymbol{W}_0,\boldsymbol{\Theta},\boldsymbol{X},\boldsymbol{X}_r) - \frac{1}{\rho_1}\sum_{m=1}^{M}\|\boldsymbol{Q}_m - \tilde{\boldsymbol{H}}_{i,m}\|_F^2 - \frac{1}{\rho_2}\sum_{m=1}^{M}\|\boldsymbol{q}_m - \tilde{\boldsymbol{h}}_{t,m}\|_F^2 \tag{76}$$

$$s.t.\quad 0 \le X_m^n \le X_{m+1}^n - \delta, m = 1 \tag{77}$$

$$X_{n,m-1} + \delta \le X_{n,m} \le X_{n,m+1} - \delta, \quad 2 \le m \le M-1, \tag{78}$$

$$X_{n,M-1} + \delta \le X_{n,M} \le L, \quad m = M. \tag{79}$$

The above problem is a one-dimensional bounded optimization, which can be efficiently solved through cell search. Specifically, the continuous variable $X_{n,m}$ is first subjected to a coarse uniform search over Q points within the feasible region to identify the initial optimal position. Subsequently, a local fine grid is constructed centered at this point, which is partitioned into Q_{fine} grid points, and a secondary search is performed over the fine grid to obtain the local optimal solution.

4) Update of the Transmit Antenna Position Variable $\mathbf{X}_r$

With $\mathbf{Q}$, $\{\mathbf{Q}_m\}_{m=1}^M$, and $\mathbf{X}$ fixed, the subproblem with respect to the position variable $\mathbf{X}_r$ can be formulated as

$$\max_{\boldsymbol{X},\boldsymbol{X}_r} -\frac{1}{\rho_3}\sum_{m=1}^{M}\left\|q_{r,m} - \tilde{h}_{r,m}\right\|_F^2 \tag{80}$$

$$\text{s.t.} \quad [\mathbf{X}_r]_{n,m} \in \mathcal{X}_r \tag{81}$$

For the position optimization of the receive waveguide antennas, the same adaptive one-dimensional search strategy as employed for the transmit waveguide is adopted. Since the receive waveguide features a single-antenna structure, the one-dimensional position search can be performed directly in sequential antenna order while keeping all other positions fixed, seeking the position within the feasible interval that maximizes the objective function.

IV. SIMULATION EXPERIMENT

A. SIMULATION PARAMETER SETTING

This paper considers a near-field and far-field integrated ISAC system with cooperative assistance from PASS and multiple RIS. The base station (BS) is located at $(0, 0)$, operating at a carrier frequency of 28 GHz, and is equipped with N' receive antennas. The service coverage area of the system is situated in the X-Y plane, where both communication users and sensing targets are uniformly distributed within this region.

The PASS consists of $N = 4$ RF feedlines, with each waveguide capable of accommodating up to $M = 4$ pinching antennas (PAS). The minimum inter-antenna spacing is set to $d_{\min} = 10$ meters, the effective refractive index is n_e, and the available track length is L_{WG} meters. The vertical height of the PASS is configured as h_{PA} meters, maintaining a horizontal distance of $D_{\text{BS}}= 5$ meters from the BS.

The system deploys L RIS, each comprising R active reflecting elements, with their positions configured at $(10, 6)$,$(16, 0)$, and $(10, -6)$, respectively. These RIS are deployed to provide reflection link enhancement for farfield communication users located beyond the near-field coverage range of the PASS. The transition between these regions is dynamically calculated based on the system's 28 GHz operating frequency, ensuring the far-field users are strictly located beyond the Rayleigh distance of the PASS aperture.

The system simultaneously serves multiple types of users, including 4 near-field communication users, 3 far-field communication users, and 1 near-field sensing target. The receiver noise power for both communication users and the BS is set to -90 dBm. The maximum transmit power for both the BS and RIS is 30 dBm, and the power allocation factor for the PA in the PASS is configured as η. The minimum SINR threshold required for the sensing target is set to $\tau = 10$ dB.

B. BASELINE PROTOCOL

In order to evaluate the performance of the proposed joint optimization system, some baseline schemes have been designed for comparison purposes. In an attempt to provide a fair level of comparison and ensure the statistical validity of the presented results, each scheme has been evaluated for a total of 100 runs on the same channel conditions.

TABLE 1. Element-wise one-dimensional search procedure for optimizing the transmit waveguide antenna positions.

Algorithm 1: Per-Element Update Algorithm for Solving Problem (74), (75)

Input: Initial feasible PASS deployment variable set $\mathbf{X}^{(0)} = \{x_m^{n(0)}, \forall m, n\}$, convergence tolerance $\epsilon_2 > 0$

Output: Optimized PASS antenna position set $\mathbf{X}^*$

1: **Initialize:** Iteration index $t = 0$
2: **repeat**
3:     **for** $n = 1$ to N **do**
4:         **for** $m = 1$ to M **do**
5:             Update $x_m^{n(t+1)}$ by solving problem (76)
6:         **end for**
7:     **end for**
8:     Obtain the updated variable set $\mathbf{X}^{(t+1)}$ based on Steps 3-7, and set $t = t + 1$
9: **until** $\mathbf{X}^{(t+1)} - \mathbf{X}^{(t)} \le \epsilon_2$
10: **return** Optimized antenna position set $\mathbf{X}^* = \mathbf{X}^{(t)}$.

TABLE 2. Penalty-based iterative algorithm for optimizing the PASS antenna positions.

Algorithm 2: Penalty Function Method for Solving Problem (P3)

Input: Convergence tolerance $\epsilon_3^1 > 0$ for AO, convergence tolerance $\epsilon_3^2 > 0$ for penalty iteration, penalty factor ρ, update coefficient $\mu < 0$

Output: Optimized variables $\mathbf{Q}^*$, $\mathbf{Q}_m^*$, $\mathcal{X}^*$, $\mathcal{X}_r^*$

1: **Initialize:** All feasible auxiliary matrices $\mathbf{Q}^{(0)}$, $\mathbf{Q}_m^{(0)}$ and PA deployment variable set $\mathcal{X}^{(0)}$, $\mathcal{X}_r^{(0)}$ for m, iteration index $t = 0$
2: **repeat**
3:     **repeat**
4:         Given $\mathbf{Q}_m^{(t)}$, $\mathbf{q}_m^{(t)}$, $\bar{q}_{r,m}^{(t)}$ and $\mathcal{X}^{(t)}$, $\mathcal{X}_r^{(t)}$, update $\mathbf{Q}^{(t+1)}$, $\mathbf{q}_{s,T}^{(t+1)}$, $\tilde{q}_r^{(t+1)}$ by solving problem (65)
5:         Given $\mathbf{q}_{s,T}^{(t+1)}$, $\tilde{q}_r^{(t+1)}$ and $\mathcal{X}^{(t)}$, $\mathcal{X}_r^{(t)}$, update $\mathbf{Q}_m^{(t+1)}$, $\mathbf{q}_m^{(t+1)}$, $\bar{q}_{r,m}^{(t+1)}$ based on equations (71)-(73)
6:         Given $\mathbf{Q}^{(t+1)}$, $\mathbf{q}_{s,T}^{(t+1)}$, $\tilde{q}_r^{(t+1)}$ and $\mathbf{Q}_m^{(t+1)}$, $\mathbf{q}_m^{(t+1)}$, $\bar{q}_{r,m}^{(t+1)}$, update $\mathcal{X}^{(t+1)}$, $\mathcal{X}_r^{(t)}$ by solving problem (77) via Algorithm 1
7:         $t \leftarrow t + 1$
8:     **until** The objective function increment of problem (P3) is less than ϵ_3^2
9:     $\rho \leftarrow \mu\rho$
10: **until** AO iteration progress is less than ϵ_3^1
11: **return** Optimized variables $\mathbf{Q}^* = \mathbf{Q}^{(t)}$, $\mathbf{Q}_m^* = \mathbf{Q}_m^{(t)}$, $\mathcal{X}^* = \mathcal{X}^{(t)}$, $\mathcal{X}_r^* = \mathcal{X}_r^{(t)}$

TABLE 3. Overall AO algorithm for joint optimization of beamforming, active RIS reflection, and PASS placement.

Algorithm 3: Overall AO Algorithm for Solving Problem (29)

Input: Convergence tolerance $\epsilon_4 > 0$, PASS position convergence tolerance $\epsilon_5 > 0$

Output: Optimized variables $\mathbf{W}^*$, $\mathbf{W}_0^*$, $\mathbf{X}^*$, $\mathbf{X}_r^*$, $\mathbf{\Theta}^*$

1: **Initialize:** PA deployment variable set $\mathbf{X}^{(0)}$, $\mathbf{X}_r^{(0)}$, iteration index $t = 0$
2: **repeat**
3:     Given $\mathbf{W}^{(t)}$ and $\mathbf{W}_0^{(t)}$, update $\mathbf{X}^{(t+1)}$, $\mathbf{X}_r^{(t+1)}$ via Algorithm 2
4:     **repeat**
5:         Given $\mathbf{X}^{(t)}$, $\mathbf{X}_r^{(t)}$ and $\mathbf{\Theta}$, update $\mathbf{W}^{(t+1)}$ and $\mathbf{W}_0^{(t+1)}$ by solving problem (P1)
6:         Given $\mathbf{W}^{(t+1)}$, $\mathbf{W}_0^{(t+1)}$ and $\mathbf{X}^{(t+1)}$, $\mathbf{X}_r^{(t+1)}$, update $\mathbf{\Theta}$ by solving problem (P2)
7:     **until** The relative change of $\mathbf{W}^{(t+1)}$, $\mathbf{W}_0^{(t+1)}$, $\mathbf{\Theta}$ between two consecutive iterations is less than ϵ_4
8:     $t \leftarrow t + 1$
9: **until** The relative change of $\mathbf{X}^{(t+1)}$, $\mathbf{X}_r^{(t+1)}$ between two consecutive iterations is less than ϵ_5
10: **return** Optimized variables $\mathbf{W}^* = \mathbf{W}^{(t)}$, $\mathbf{W}_0^* = \mathbf{W}_0^{(t)}$, $\mathbf{X}^* = \mathbf{X}^{(t)}$, $\mathbf{X}_r^* = \mathbf{X}_r^{(t)}$, $\mathbf{\Theta}^* = \mathbf{\Theta}^{(t)}$

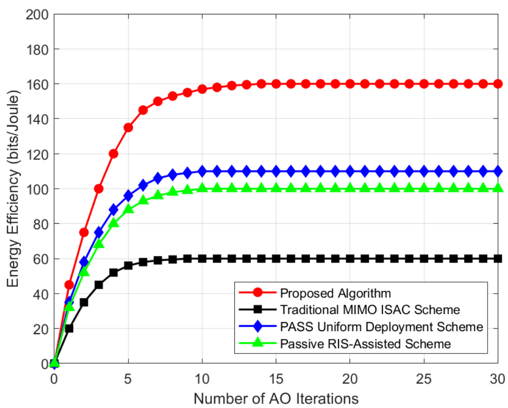

FIGURE 2. Communication energy efficiency versus the number of AO iterations.

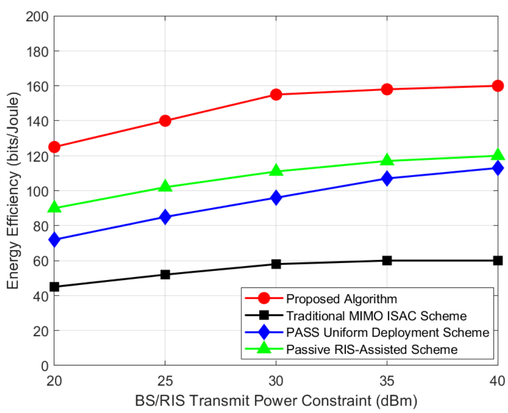

FIGURE 3. Communication energy efficiency versus the BS/RIS transmit-power budget.

Conventional MIMO ISAC Scheme: In the traditional MIMO ISAC scheme, the BS is equipped with a fixed-position uniform linear array (ULA) with $N = 4$ transmit antennas, replacing the flexible PASS waveguide structure. The RIS configuration remains a 2×2 active element array to ensure a fair comparison of the antenna deployment gain. For signal processing, the MIMO baseline employs joint beamforming for simultaneous radar-communication but lacks the degrees of freedom provided by antenna position optimization on the waveguides. The same total power budget P_{BS} and active RIS power P_{A} are applied to this scheme to validate the specific advantages of the PASS-based ISAC architecture.

PASS Uniform Deployment Scheme: In the baseline scheme, the pinching antennas are arranged along the waveguides. The beamforming vector and reflection vector algorithms are not changed.

Passive RIS-assisted scheme: A passive RIS is used to substitute the RIS in the scenario of the far-field users in this baseline scheme, leaving the optimization schemes of the PASS and beamforming schemes unchanged.

Next, we examine the convergence speed of the proposed algorithm. As shown in Fig. 2, the proposed joint PASS-RIS optimization approach can achieve a very fast convergence speed to a steady state within the first 15 iterations with a final energy efficiency of about 160 bit/J, respectively, demonstrating a huge performance gain over all the competing methods. This clearly indicates the effectiveness of the joint design among the positions of the waveguides, the configurations of the PASS arrays, and the active RIS gain components. Compared with the proposed joint approach using the PASS arrays in a uniform deployment configuration and the passive RIS-based system employing the assistance of the PASS arrays, we can see from the convergence performance in Fig. 2 they can achieve a faster convergence speed in the first few iteration cycles but with a maximum energy efficiency of about 110 bit/J and 100 bit/J, respectively. This is reasonable since these two systems cannot search for the PA positions and offer active RIS amplification gains at the same time but can achieve improved convergence speed mainly because of the simplicity of PASS deployment configuration and passive RIS phase change control assistance without the need for amplification gain support for far-field users with very strong path-attenuated signal components. The existing MIMO-Integrated-ISAC scenario with a convergence value of about 60 bit/J can be less effective in many aspects because the system does not enhance the near-field regions with the transmission assistance of the PASS arrays using the ISAC technique.

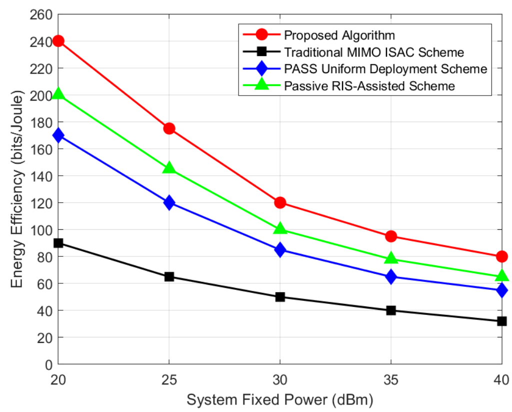

FIGURE 4. Comparison of communication energy efficiency under different fixed system transmit-power settings.

Furthermore, the effect of the transmit power constraint on the energy efficiency of the proposed system is also analyzed. As shown in Fig. 3, with the increase of the transmit power from 20 dBm to 30 dBm, it is observed that the energy efficiency of the proposed scheme and all the baselines remarkably improves. This is due to the better communication link quality offered by the higher transmit power, thus improving the communication rate, which also results in an increasing trend in the energy efficiency in the initial stage with an increase in power. However, with the further increase in transmit power from 30 dBm to 40 dBm, it is observed that the energy efficiency of all schemes except the passive RIS-assisted one tends to be saturated. The reasons are as follows: The proposed PASS-RIS joint scheme, the PASS uniform deployment scheme, and the MIMO scheme are already at the approximately optimal point in the EE vs. power curve around 30 dBm; higher transmit power provides only marginal gains in communication rate but substantially increases the energy consumption, thus reaching a saturated point in the energy efficiency gains. The passive RIS scheme is restricted by the path-attenuation factor due to the lack of active gain; thus, higher transmit power from the BS is needed to compensate for the link loss in the communication between the RIS and the communication users in the far-field region, thus gaining some performance improvements in the high-power region. The proposed scheme provides the supreme performance in the energy efficiency performance based on the constraints on various powers, particularly in the low-to-medium region in the transmit power constraint regime.

Fig. 4 depicts the effect of fixed power consumption on system EE. It can be seen that as an increasing value of fixed power consumption, all algorithm schemes reveal a decreasing trend for EE due to the reduced weightage of effective RP to total power consumption, and the performance difference among different schemes gradually becomes smaller. When moving to the low fixed power consumption area, effective power plays a larger role, and hence, the performance gain provided by joint optimization can be completely enjoyed by all schemes, which helps to result in a substantial higher EE for our proposed scheme. Observing that increasing fixed power consumption leads to a slow decline among all schemes, as it continuously counteracts the rising system overhead, hence, all schemes are moving towards a converged level as compared to base schemes. However, our proposed PASS-active RIS joint optimization scheme all along maintains its superiority by providing the highest EE, as our scheme has effective access to both PASS's ability to improve the link quality and active RIS gain to reinforce an effective channel and stronger suppression to affiliated interferers, hence, its superior performance advantages are well proven over different levels of fixed power consumption conditions. The base scheme without PASS performs poorly, especially for low fixed power consumption, as its EE badly lags behind other schemes, which clearly shows that it is impractical to only leverage traditional BF to improve channel quality by compensating path loss, but adding PASS helps to play a vital support role to reinforce effective gain during adverse channel conditions.

Fig. 5 shows the effect of the number of attachable antennas per waveguide M on the system energy efficiency for each of the three methods and the method without PASS. From this figure, it can be noted that with the increment of M, the EE of all three methods increases; meanwhile, the EE of the method without PASS remains constant. From the methods with PASS, the joint PASS-RIS beamforming optimization approach always shows the best performance with the maximum improvement margin. This method combines the local gain control of PASS and the far-field compensation gain of active RIS with the beamforming

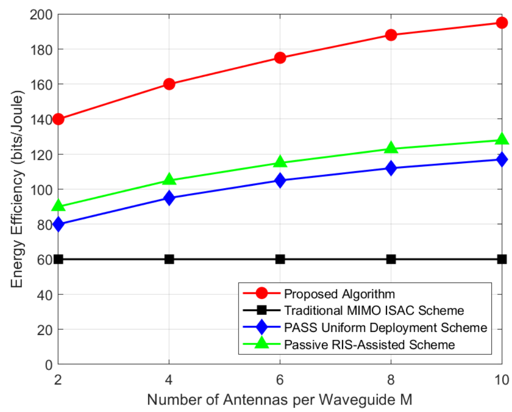

FIGURE 5. Communication energy efficiency versus the number of antennas deployed on each waveguide.

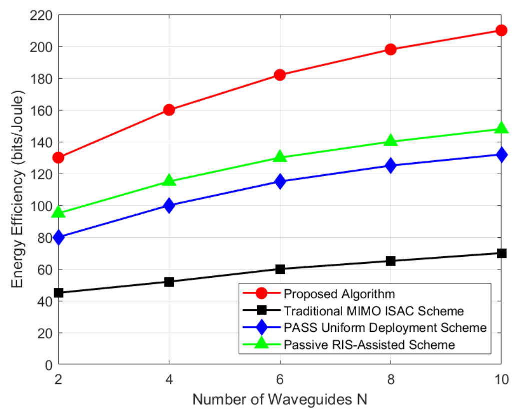

FIGURE 6. Communication energy efficiency versus the number of waveguides.

gain of the digital baseband.

Therefore, the optimal performance is realized with different values of M. Conversely, the performance of the scheme with fixed PASS locations also experiences some gains with the increase in M, but because of the lack of the ability to change the locations using PASS, it experiences a relatively small EE gap of improvement compared to the optimizable case. The simultaneous optimization technique using the passive RIS relies on the PASS optimization technique, which has the capability of adaptively changing the locations of the antennas with the rise in the number of antennas to fully capture the passive reconfigurable gains of PASS. Hence, it offers a better performance compared to the original technique using fixed locations of PASS. The traditional MIMO technique does not depend on the number of antennas, and hence there is no EE gain derived from using an increased number of antennas.

Fig. 6 above outlines the relationship graphics among energy efficiency and the total number of waveguides N. From the graphics, it is noted that increasing the total number of waveguides N will lead to a prominent improvement in the EE for all four schemes. Of the four schemes, the EE improvement for the joint optimal method remains the largest, with the improvement rate becoming faster compared with the other three schemes with the increase in the total number of waveguides. The reason lies in the fact that the more waveguides there are, the more enhanced the energy focusing capability will be in the service area, leading to the expansion of the adjustment scope for PASS and RIS, which will further lead to enhanced communication quality and sensing quality during the adjustment process. The passive RIS combined with PASS will benefit from the increase in the total number of waveguides, with the EE increasing steadily along with the rise in the total number of waveguides. The method with fixed PASS locations will improve EE as well. However, since the method has limited spatial adjustment capability, the degree of improvement remains moderate. The method without PASS will not benefit from the increase in the total number of waveguides. However, increasing the total number of waveguides will bring changes to the total number of base substation antennas, leading to improvement in EE with the smallest improvement margin. It should be noted that compared with the improvement margin caused by increasing the total number of waveguides in Fig. 5, the improvement margin by increasing M in Fig. 6 will become relatively small. This is because increasing N expands

the overall controllable aperture of PASS and enhances the spatial degrees of freedom, thereby significantly improving the equivalent channel. On the other hand, the increase in the value of M merely optimizes the set of adjustable discrete locations in a given waveguide, hence improving the surrounding array gain but marginally improving the overall channel. Additionally, the simultaneous increment of the value of N not only increases the dimensionality of the digital beamforming vector in the base station but also gives the system more spatial degrees of freedom. This enables a faster improvement in the overall EE performance.

V. CONCLUSION

This study investigates a novel Integrated Sensing and Communication (ISAC) downlink system that leverages the cooperative synergy between Pinching Antenna Systems (PASS) and multiple active Reconfigurable Intelligent Surfaces (RIS) to facilitate high-precision data acquisition and connectivity across flexible, intelligent surfaces. By addressing the challenge of enhancing spectral and energy efficiency (EE) in 6G wireless networks, the research proposes a joint optimization framework to maximize communication energy efficiency while adhering to strict sensing Signal-to-Noise Ratio (SNR) and power budget constraints.

The complex optimization problem is effectively decoupled into three tractable sub-problems—PASS antenna positioning, digital beamforming, and active RIS reflection matrix design—and solved using an alternating optimization strategy involving fractional programming and penalty function methods. Simulation results demonstrate that the proposed joint approach achieves a steady-state energy efficiency of approximately 160 bit/J, significantly outperforming baseline schemes such as traditional MIMO (60 bit/J), uniform PASS deployment (110 bit/J), and passive RIS-assisted systems (100 bit/J).

AUTHOR CONTRIBUTIONS

Feiyang Yu designed, collected and analyzed the data, and drafted the manuscript. Feiyang Yu conducted the study, critically revised the manuscript for important intellectual content, and gave final approval of the version to be published. Feiyang Yu participated fully in the work, take public responsibility for appropriate portions of the content, and agreed to be accountable for all aspects of the work in ensuring that questions related to the accuracy or integrity of any part of the work are appropriately investigated and resolved.

CONFLICTS OF INTEREST

The authors declare no conflict of interest.

FUNDING

This research received no external funding.

ACKNOWLEDGEMENTS

Not applicable.

REFERENCES

[1] Y. Liu, X. Liu, X. Mu, et al., “Reconfigurable Intelligent Surfaces: Principles and Opportunities[J],” IEEE Communications Surveys & Tutorials, 2021, no. 3, doi: 10.1109/COMST.2021.3077737.
[2] Zhu Lipeng, Ma Wenyan, and Zhang Rui, “Movable Antennas for Wireless Communication: Opportunities and Challenges[J],” IEEE Communications Magazine, 2024, doi: 10.1109/MCOM.001.2300212.
[3] K. K. Wong, A. Shojaeifard, K. F. Tong, et al., “Fluid Antenna Systems[J],” IEEE Transactions on Wireless Communications, 2021, no. 3, doi: 10.1109/TWC.2020.3037595.
[4] C. Huang, R. Mo, and C. Yuen, “Reconfigurable Intelligent Surface Assisted Multiuser MISO Systems Exploiting Deep Reinforcement Learning[J],” IEEE Journal on Selected Areas in Communications, 2020, no. 38-8, doi: 10.1109/jsac.2020.3000835.
[5] P. Wang, J. Fang, X. Yuan, et al., “Intelligent Reflecting Surface-Assisted Millimeter Wave Communications: Joint Active and Passive Precoding Design[J],” IEEE Transactions on Vehicular Technology, 2020, vol. 99, pp. 1–1, doi: 10.1109/TVT.2020.3031657.
[6] C. Huang, A. Zappone, G. C. Alexandropoulos, et al., “Reconfigurable Intelligent Surfaces for Energy Efficiency in Wireless Communication[J],” IEEE Transactions on Wireless Communications, vol. 18, no. 99, pp. 4157–4170, 2019, doi: 10.1109/TWC.2019.2922609.
[7] X. Hu, C. Liu, M. Peng, et al., “IRS-Based Integrated Location Sensing and Communication for mmWave SIMO Systems[J],” IEEE Transactions on Wireless Communications, 2023, no. 6, p. 22, doi: 10.1109/TWC.2022.3223428.
[8] X. Wang, Z. Fei, Z. Zheng, et al., “Joint Waveform Design and Passive Beamforming for RIS-Assisted Dual-Functional Radar-Communication System[J],” IEEE Transactions on Vehicular Technology, vol. 70, no. 5, pp. 5131–5136, 2021, doi: 10.1109/TVT.2021.3075497.
[9] Z. Zhang, L. Dai, X. Chen, et al., “Active RIS vs. Passive RIS: Which Will Prevail in 6G?[J],” 2021, doi: 10.48550/arXiv.2103.15154.
[10] Q. Zhang, H. Wu, H. Li, et al., “Joint Location and Beamforming Design for Energy Efficient STAR-RIS-Aided ISAC Systems[J],” IEEE Communications Letters, 2025, no. 1, p. 29, doi: 10.1109/LCOMM.2024.3503754.
[11] W. Ma, P. Zhang, J. Ye, et al., “Joint Antenna Selection and Beamforming Design for Active RIS-aided ISAC Systems[J],” 2025, doi: 10.1109/JIOT.2025.3560128.
[12] Z. Zhang, Z. Wang, X. Mu, et al., “Integrated Sensing and Communications for Pinching-Antenna Systems (PASS)[J],” 2025, doi: 10.1109/LCOMM.2025.3619778.

[13] L. I. Conggai, F. Liu, L. I. Yingying, et al., "Energy Efficiency Maximization for Active RIS Switcher Assisted MISO Systems[J]," IEICE Transactions on Fundamentals of Electronics, Communications and Computer Sciences, 2024, doi: 10.1587/transfun.2024eal2060.
[14] K. Shen and W. Yu, "Fractional Programming for Communication Systems–Part I: Power Control and Beamforming[J]," IEEE Transactions on Signal Processing, pp. 1–1, 2018, doi: 10.1109/TSP.2018.2812733.